pubs.acs.org/acschemicalbiology

Articles

Conditional Antisense Oligonucleotides Triggered by miRNA

Jiahui Zhang, Radhika Sharma, Kitae Ryu, Patrick Shen, Khalid Salaita,* and Hanjoong Jo*

Cite This: https://doi.org/10.1021/acschembio.1c00387

Read Online

ACCESS | Metrics & More | Article Recommendations | Supporting Information

ABSTRACT: Antisense oligonucleotides (ASOs) are single-stranded short nucleic acids that silence the expression of target mRNAs and show increasing therapeutic potential. Since ASOs are internalized by many cell types, both normal and diseased cells, gene silencing in unwanted cells is a significant challenge for their therapeutic use. To address this challenge, we created conditional ASOs that become active only upon detecting transcripts unique to the target cell. As a proof-of-concept, we modified an HIF1α ASO (EZN2968) to generate miRNA-specific conditional ASOs, which can inhibit HIF1α in the presence of a hepatocyte-specific miRNA, miR-122, via a toehold exchange reaction. We characterized a library of nucleic acids, testing how the conformation, thermostability, and chemical composition of the conditional ASO impact the specificity and efficacy in response to miR-122 as a trigger signal. Optimally designed conditional ASOs demonstrated knockdown of HIF1α in cells transfected with exogenous miR-122 and in hepatocytes expressing endogenous miR-122. We confirmed that conditional ASO activity was mediated by toehold exchange between miR-122 and the conditional ASO duplex, and the magnitude of the knockdown depended on the toehold length and miR-122 levels. Using the same concept, we further generated another conditional ASO that can be triggered by miR-21. Our results suggest that conditional ASOs can be custom-designed with any miRNA to control ASO activation in targeted cells while reducing unwanted effects in nontargeted cells.

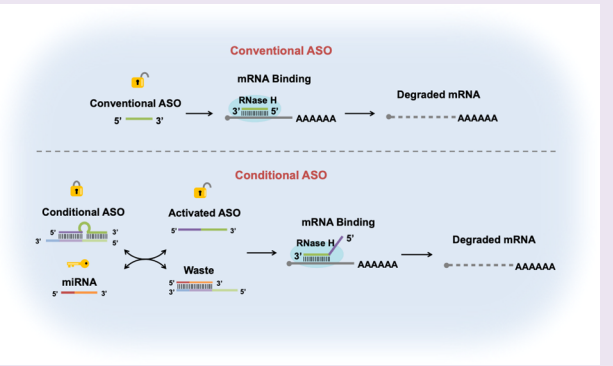

INTRODUCTION

Antisense oligonucleotides (ASOs) are single-stranded synthetic nucleic acids that can cleave target mRNAs through Watson−Crick−Franklin base pairing and recruitment of RNase H.[1−3] Since ASOs are relatively easy to design and synthesize against virtually any mRNA of interest, they have become promising therapeutics.[4] Despite these advantages, the clinical success of ASOs was initially hindered by their low efficacy due to nuclease susceptibility and limited cell entry. These problems have been overcome with the advent of chemical modifications that protect against nucleases (e.g., the gapmer design)[5] and conjugation strategies.[6] Currently, a grand challenge in ASO therapeutics pertains to reducing undesired adverse effects by delivering them specifically to the desired cell types or tissues. ASOs delivered systemically[7,8] or locally[9] are taken up by various cell types, resulting in intended effects in target cells while concomitantly inducing unintended effects in bystander cells. Thus, developing new strategies to render the ASOs active only in target cells but remain inactive in nontarget cells is crucial.

To provide cell- and tissue-specificity for ASOs, several approaches, including photocaging, lipid nanocarriers, and ligand conjugations, have been developed. However, they continue to have shortcomings in target cell-specific delivery. Photocaging[10,11] is limited by tissue penetration and potential cytotoxicity of UV light. Lipid nanocarriers with specific tissue tropism have shown the potential for tissue-specific delivery, but it is unclear if they can provide specificity of cell subtypes within tissues.[12,13] Tissue-targeted ligand conjugation, such as GalNAc-conjugated siRNA-targeting aminolevulinic acid synthase 1 (ALAS1) mRNA, has been successful.[14,15] This ligand-mediated specific cellular uptake strategy can be successful when the target cell type displays unusually high expression levels of a surface marker. However, unique surface markers are not available for many target cells. In contrast, it is much easier to identify intracellular markers such as transcripts or proteins that specifically change in target cells or tissues. Therefore, using intracellular species such as microRNAs (miRNAs) and mRNAs to control the activity of ASOs may expand the targeting competency to a broad range of pathophysiological conditions.[16,17]

HIF1α is a master transcription factor and plays important roles in both normal physiology and pathobiological

Received: May 21, 2021
Accepted: October 4, 2021

conditions. HIF1α not only regulates the physiological processes such as angiogenesis, wound healing, and acute injury repair but is also involved in various diseases, including cancer and cardiovascular diseases.[18−24] Thus, systemic inhibition of HIF1α may lead to adverse side effects, and conditional regulation of HIF1α in targeted cell types could be beneficial. EZN2968 is a single-stranded ASO with locked nucleic acid (LNA) modifications, which specifically and effectively inhibits HIF1α mRNA and tumor growth.[25] However, EZN2968 is not widely used in the clinic, in part, due to its potential side effects. Therefore, we aimed in this study to generate a conditional EZN2968 ASO, which can be activated only in cells expressing target miRNA.

MicroRNA is a key regulator of gene expression, with its expression dynamically changing under various pathophysiological conditions.[26−28] Also, some miRNAs show cell-type specific expression patterns. For example, miR-122 is a highly specific miRNA expressed in hepatocytes,[29,30] making it ideal to test the concept of miRNA-triggerable ASOs. Also, miR-21 expression is increased in numerous cancer and cardiovascular disease conditions. Therefore, here, we first used miR-122 to test the proof-of-concept of conditional EZN2968 triggered by miR-122. Then, we used another miRNA, miR-21, to test if the miRNA-regulated ASO concept can be applied in general.

We hypothesized that the single-stranded EZN2968 activity could be concealed by hybridizing it with a complementary sequence (locking strand) to make a double strand (duplex). To control the dehybridization of the EZN2968 duplex in response to miR-122, we added the complementary sequence of miR-122 to the locking strand. We further hypothesized that dehybridization of the duplex will help to regain the ASO activity, which can be achieved via toehold-mediated displacement or exchange reaction[31] triggered by miR-122. To test the hypothesis, we first modified EZN2968 to generate and characterize a library of conditional ASOs. The library was tested to identify the design features that result in the most selective triggering of EZN2968. We investigated the role of duplex architecture, including the length and spatial arrangement of single- and double-stranded domains, thermostability, and chemical composition of the conditional EZN2968. Then, we demonstrated activation of the conditional EZN2968 by both a synthetic miR-122 mimic and endogenous miR-122 in vitro. Further, we demonstrated the modularity of the design by generating another conditional EZN2968 using miR-21 as a trigger miRNA.

MATERIALS AND METHODS

Materials. All oligonucleotides (Tables S1−S3) and primers for quantitative real-time polymerase chain reaction (RT-qPCR) (Table S4) were custom synthesized by Integrated DNA Technologies. A Direct-zol RNA Miniprep Kit (Cat. #: R2052) was acquired from Zymo Research. An miScript II RT Kit (Cat. #: 218161) and miScript Primer Assays (miR-122: Cat. #: MS00003416; RNU6: Cat. #: MS00033740) were acquired from QIAGEN. An Oligofectamine Transfection Reagent (Invitrogen, Cat. #: 12252011), a High-Capacity cDNA Reverse Transcription Kit (Applied Biosystems, Cat. #: 4368813), and PerfeCTa SYBR Green FastMix Reaction Mixes (QuantaBio, Cat. #: 95073) were acquired from ThermoFisher Scientific. A luciferase assay kit (Cat. #: E4550) was acquired from Promega. HIF1α antibody is purchased from Bethyl Laboratories (Cat. #: A300-286A). β-actin antibody is purchased from Santa Cruz Biotechnology (Cat. #: sc-47,778). Goat antimouse IgG HRP (Cat. #: 10004302) and goat antirabbit IgG HRP (Cat. #: 10004301) were purchased from Cayman Chemical Company. Ambion's Anti-miR miRNA Inhibitor (Cat. #: AM17000) for miR-122 was purchased from ThermoFisher Scientific. The U373 cell line was purchased from Sigma-Aldrich (Cat. #: 08061901).

Displacement Assay in Buffer. Modified conditional EZN2968 ASOs (11.1 nM) labeled with a Cy5/quencher pair in 90 μL of PBS were preincubated at 37 °C in a 96-well plate. Then, 10 μL of 1 μM mRNA mimic or miRNA mimic was added into each well and mixed briefly. The final concentrations of conditional EZN2968 ASOs and mRNA/miRNA mimic were 10 and 100 nM, respectively. The fluorescence intensity (Ex/Em = 630/670 nm) was immediately measured with a Bio-Tek Synergy H1 microplate reader at 37 °C for 2 h with an interval of 15 min. To determine percentage displacement, a 10 nM Cy5-labeled partial miR-122-EZN2968 (pM-EZN) strand was used as a positive control, whose fluorescence intensity represents 100% activation.

Cell Culture. HeLa cells (ATCC) and LN229-V6R-Luc cells (human glioma cell line expressing HIF1a reporter luciferase)[32] were maintained in Dulbecco's modified Eagle medium (DMEM) containing 4.5 g/L glucose, 10% (v/v) fetal bovine serum (FBS), penicillin (100 U/mL), and streptomycin (100 mg/mL) at 37 °C under a humidified atmosphere of 5% CO_2. U373 cells (Sigma-Aldrich) were maintained in DMEM containing 1 g/L glucose, 10% (v/v) FBS, penicillin (100 U/mL) and streptomycin (100 mg/mL), 1% NEAA, 1 mM sodium pyruvate, and 2 mM L-glutamine at 37 °C under a humidified atmosphere of 5% CO_2. Huh7 cells (provided by Dr. Arash Grakoui's Lab at Emory University) were maintained in DMEM containing 4.5 g/L glucose, 10% (v/v) FBS, penicillin (100 U/mL), and streptomycin (100 mg/mL) at 37 °C under a humidified atmosphere of 5% CO_2.

T_m Measurement. The melting temperature (T_m) of conditional EZN2968 was measured using the dequenching of the dye due to separation of the Cy5-labeled pM-EZN strand from the quencher-labeled locking strand. The fluorescence of 100 nM conditional EZN2968 duplex in PBS was measured with a LightCycler 96 instrument as a function of temperature. The temperature was ramped from 45 to 95 °C at a rate of 0.04 °C/s, and 25 measurements were performed at each °C. T_m was determined as the temperature that generates a half-maximal fluorescence increase in the fitted curves.

Testing Spontaneous Activation of Conditional EZN2968 in HeLa and U373 Cells. U373 or HeLa cells were plated in 24-well plates with a density of 5×10^4 cells/well the day before the experiment. The 10 nM conditional EZN2968 was transfected into the cells using Oligofectamine according to the manufacturer's protocol (2 μL/well). After 24 h incubation, QIAZOL was then added into the wells to lyse the cells, and total RNA was isolated using a Direct-zol RNA Miniprep Kit (Zymo Research). RNA was reverse transcribed using a High-Capacity cDNA Reverse Transcription Kit (Applied Biosystems). HIF1α mRNA levels were quantified by RT-qPCR using PerfeCTa SYBR Green FastMix Reaction Mixes (QuantaBio) with a 0.25 μM concentration of custom-designed primers (Table S4) with an Applied Biosystems StepOnePlusTM real-time PCR system. The relative quantification of HIF1α mRNA levels was performed using the $\Delta\Delta$Ct method with 18 s rRNA as an internal control.

Testing Spontaneous Activation of Conditional EZN2968 in LN229-V6R-Luc Cells. LN229-V6R-Luc cells were plated in opaque 96-well plates with a density of 5×10^4 cells/well the day before the experiment. The 10 nM conditional EZN2968 was transfected into the cells using Oligofectamine (0.5 μL/well). After 4 h, the medium with serum along with IOX4 (HIF1α activator) was added to each well. The final concentration of IOX4 was 20 μM/well. After incubation for another 20 h, the luciferase assay was conducted as per the manufacturer's protocol (luciferase assay kit from Promega).

miR-122 Mimic-Triggered Activation of Conditional EZN2968 in U373 Cells. U373 cells were plated in 24-well plates with a density of 5×10^4 cells/well the day before the experiment. The 10 nM conditional EZN2968 and 500 nM miR-122 mimic were cotransfected using Oligofectamine according to the manufacturer's protocol (2 μL/well in total). Note that the transfection mixtures of the conditional EZN2968 and miR-122 mimic were prepared

https://doi.org/10.1021/acschembio.1c00387
ACS Chem. Biol. XXXX, XXX, XXX−XXX

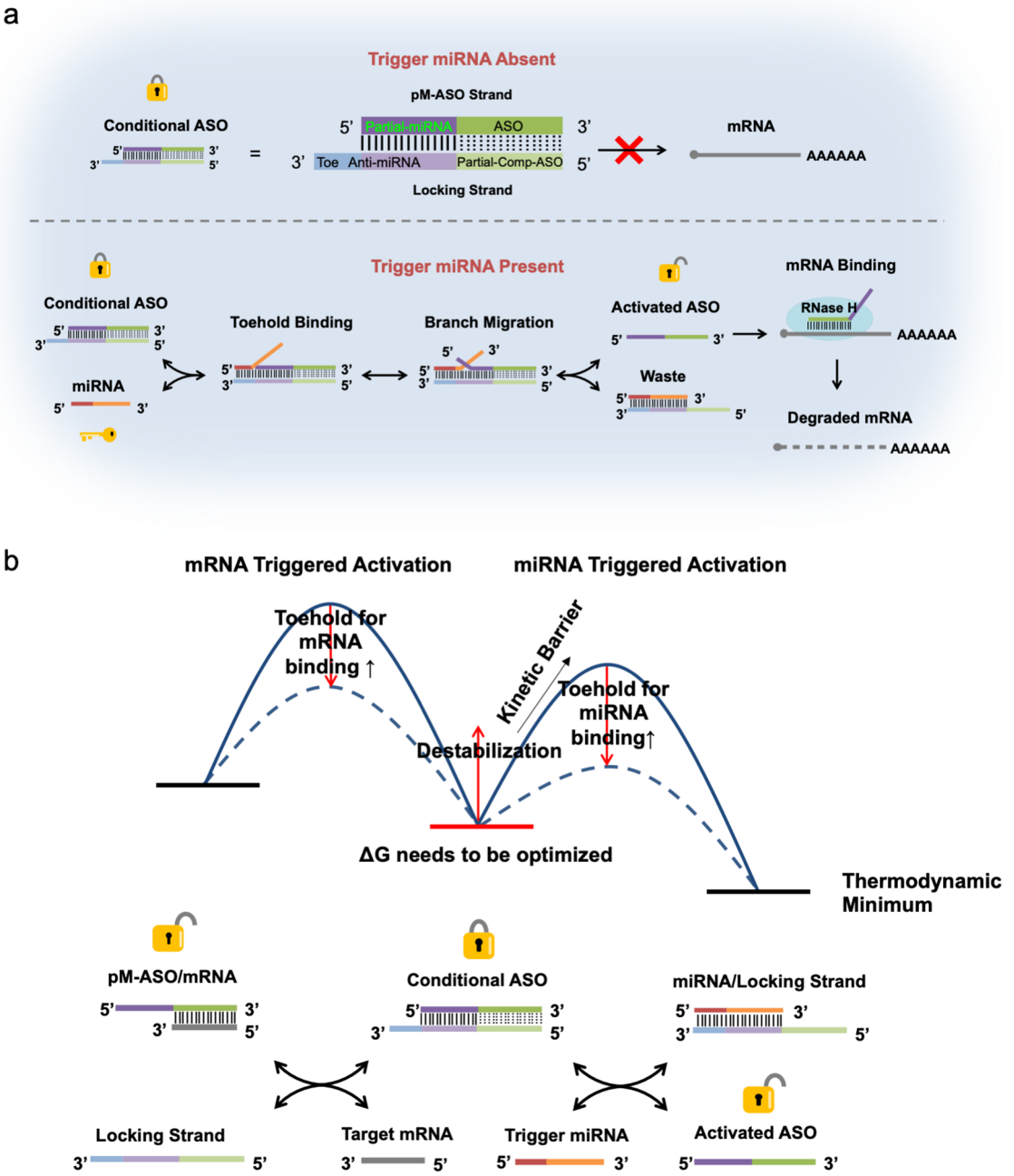

Figure 1. Scheme showing (a) design and triggering mechanism of the conditional ASO, and (b) energy diagram of conditional ASO activation. (a) Conditional ASO is formed by annealing the pM-ASO strand and the locking strand. The pM-ASO strand is the parental ASO extended with a partial miRNA sequence at its 5′ terminus. The locking stand comprises an anti-miRNA sequence and partially complementary sequence of the ASO (the dotted lines indicating partial hybridization rather than complete hybridization of the ASO domain). The mRNA-targeting ASO sequence in the conditional ASO is partially sequestered, which abolishes its binding capability to the target mRNA in the absence of the trigger miRNA. The duplex can dissociate in the presence of the trigger miRNA, exposing the mRNA-targeting ASO sequence and causing the downregulation of the target mRNA. (b) Energy diagram shows displacement of the pM-ASO strand by trigger miRNA or displacement of the locking strand by target mRNA. Conditional ASO binding to miRNA is more favorable than binding to the target mRNA when the ΔG of the miRNA/locking strand duplex is lower than that of the pM-ASO/mRNA duplex. The kinetic barrier of the reactions can be reduced by introducing the toehold in the locking strand or the ASO domain of the pM-ASO strand to facilitate miRNA or mRNA binding.

separately and added into the wells simultaneously to avoid reaction of the conditional EZN2968 and miR-122 mimic during incubation before transfection. The 10 nM conditional EZN2968-only and 500 nM miR-122 mimic-only groups were used as controls. After 24 h incubation, HIF1α mRNA levels were quantified by RT-qPCR as described above.

miR-122 Dependency of HIF1α Knockdown in Huh7 Cells. Huh7, a human hepatoma cell line, was plated in 24-well plates with a density of 10^5 cells/well the day before the experiment. Huh7 cells were transfected with 0, 100, or 500 nM anti-miR-122 using Oligofectamine and incubated for 6 h (medium with 3× serum was added 4 h after transfection). Then, 50 nM conditional EZN2968 was transfected using Oligofectamine. After another 24 h incubation, HIF1α mRNA levels were quantified by RT-qPCR as described above.

https://doi.org/10.1021/acschembio.1c00387
ACS Chem. Biol. XXXX, XXX, XXX−XXX

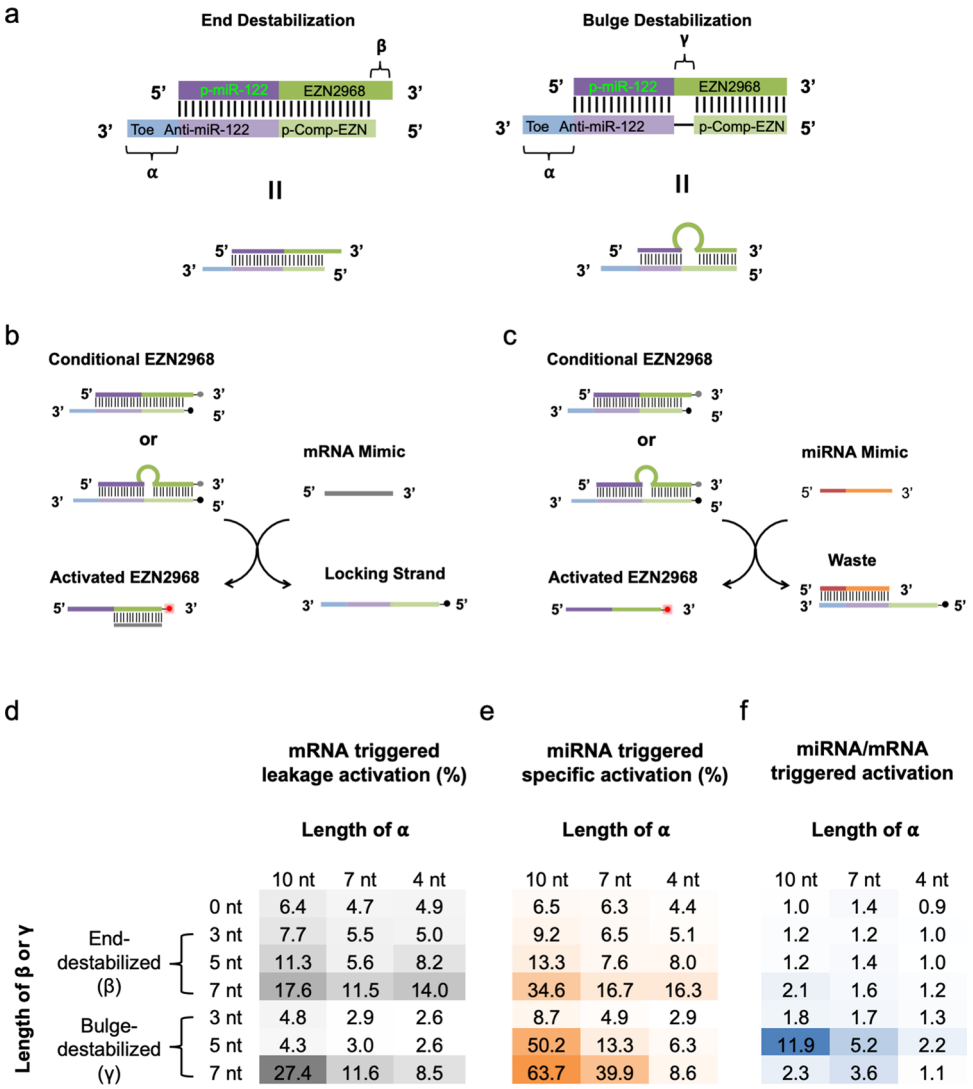

Figure 2. Design optimization of duplex conformation of conditional EZN2968. (a) Design of conditional EZN2968 with end destabilization and bulge destabilization. For end destabilization, 3−7 nt on the 5′ termini of the locking strand was removed. For bulge destabilization, 3−7 nt in the 3′ termini of the EZN2968 complementary sequence in the locking strand was removed. (b, c) Schematic description of in-buffer assay to measure (b) leakage activation of the conditional EZN2968 triggered by an HIF1α mRNA mimicking sequence, and (c) miR-122-triggered activation of the conditional EZN2968. Cy5 and the quencher were labeled on the pM-EZN strand and the locking strand separately. The annealed duplex was incubated with (b) HIF1α mRNA mimicking sequence (mRNA mimic) or (c) miR-122 mimicking sequence (mRNA mimic). The fluorescence increases due to dequenching caused by displacement were quantified. (d) 10 nM duplex was incubated with 100 nM HIF1α mRNA mimic at 37 °C for 2 h, and the fluorescence intensity of Cy5 was measured to determine the percentage of activated pM-EZN strands. n = 3. (e) 10 nM duplex was incubated with 100 nM miRNA mimic at 37 °C for 2 h, and the fluorescence intensity of Cy5 was measured to determine the percentage of activated pM-EZN strands. n = 3. (f) Ratio of miR-122-triggered displacement and mRNA-triggered displacement is shown.

Western Blot. After treatment and incubation, the cells were lysed using a lysis buffer with 50 mM Tris−HCl (pH 6.8), 10% glycerol, 2.5% SDS, 5 mM DTT, and 6 M urea supplemented with a protease inhibitor cocktail. The proteins were quantified with the BCA assay, diluted in the lysis buffer with reducing loading dye to a final protein amount of ∼10−20 μg, and boiled at 95 °C for 5 min. The proteins were separated by electrophoresis in an 8% Tris−HCl polyacrylamide gel, before transferring onto a polyvinylidene fluoride membrane. After being blocked for 1 h in 5% (w/v) nonfat milk in Tris-buffered saline with 0.1% Tween, the membranes were immunoblotted using primary antibodies against human HIF1α (1:500 dilution) or β-actin (1:3000 dilution) overnight at 4 °C. After washing, the membranes were incubated with secondary horseradish peroxide-conjugated antibody (1:5000) for 1 h at room temperature. After washing, an Immobilon Western Chemiluminescent HRP substrate was added to the membrane, and the membrane was imaged using an iBright FL1000 imaging system.

Flow Cytometry. HeLa cells or U373 cells were plated in a 12-well plate with 10^5 cells/well the day before the experiment. For testing spontaneous activation, the cells were transfected with 10 nM conditional EZN2968 labeled with a Cy5/quencher pair and incubated for 24 h. For testing miR-122-triggered activation of conditional EZN2968, the cells were cotransfected with 10 nM conditional EZN2968 and 500 nM miR-122 and incubated for 24 h. The cells were then subjected to trypsinization, washed with HBSS twice, and resuspended in HBSS for flow cytometry assessment using a CytoFLEX (Beckman Coulter) to measure the cell-associated fluorescence intensity of Cy5.

Fluorescence Lifetime Imaging (FLIM). U373 cells were plated in glass-bottom black 96-well plates with a density of 10^4 cells/well 1 day before the experiment. The cells were cotransfected with 10 nM Cy5/quencher-labeled conditional EZN2968 and 500 nM miR-122, scrambled (scr.) miR-122 or scr. 1−7 nt miR-122 using Oligofectamine and incubated for 24 h. The cells were then washed with PBS

https://doi.org/10.1021/acschembio.1c00387
ACS Chem. Biol. XXXX, XXX, XXX−XXX

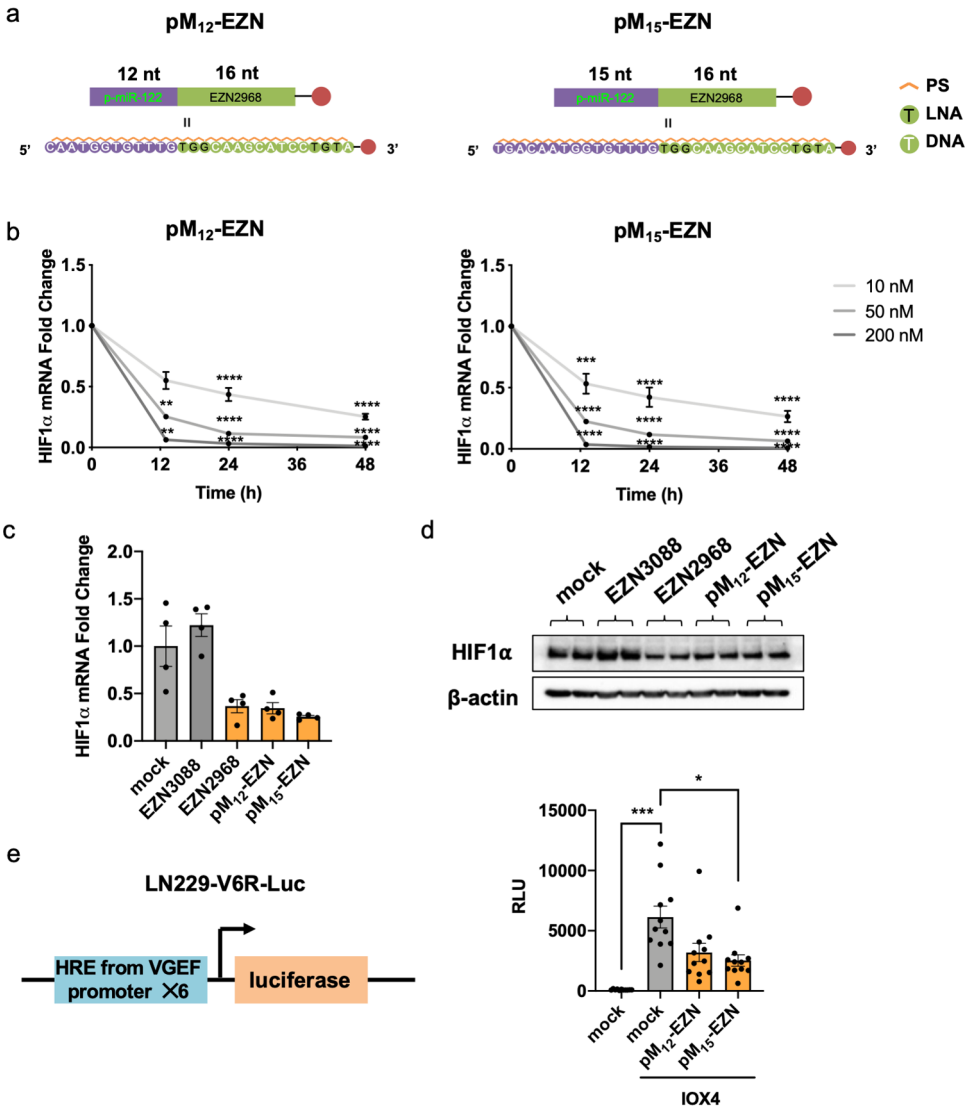

Figure 3. pM-EZN strands knock down HIF1α in a concentration- and time-dependent manner in U373 cells. (a) Design and sequences of pM-EZN strands, pM_{12}-EZN and pM_{15}-EZN. The green domain represents the original EZN2968 ASO, while the purple domain represents the partial miR-122 sequence extension. The red circle represents Cy5 dye, PS stands for phosphorothioate, and LNA stands for locked nucleic acid. (b) U373 cells were transfected with 10, 50, or 200 nM concentrations of pM_{12}-EZN or pM_{15}-EZN and incubated for 13−48 h. HIF1α mRNA levels were quantified by qPCR normalized to 18 s. ** $p < 0.01$, *** $p < 0.001$, and **** $p < 0.0001$; one-way ANOVA with Tukey's multiple comparison to the initial time point. (c, d) U373 cells were transfected with 10 nM EZN3088 (scrambled EZN2968), EZN2968, pM_{12}-EZN, or pM_{15}-EZN, and incubated for 24 h. Comparison of (c) HIF1α mRNA and (d) protein knockdown efficacy of pM_{12}-EZN, pM_{15}-EZN, and the original EZN2968. (e) LN229-V6R-Luc cells transfected with 10 nM pM_{12}-EZN or pM_{15}-EZN for 4 h were treated with IOX4 (20 μM) for another 20 h, and the luciferase assay was used to quantify HIF1α activity. The error bars represent SEM. * $p < 0.05$; *** $p < 0.001$; Brown−Forsythe and Welch ANOVA tests with Dunnett's T3 multiple comparison.

twice and fixed with 4% paraformaldehyde. After washing with PBS twice to remove fixing solution, the nucleus was stained with Hoechst 33342 for 30 min. The cells were washed with PBS another two times, and 150 μL of PBS was added to the wells before the cells were imaged. The FLIM images were analyzed using SymphoTime (PicoQuant) software. The overall fluorescence lifetime decay trace was fitted to a biexponential function through an iterative reconvolution method. The instrument response function for the iterative reconvolution analysis was measured using saturated Coomassie Blue and potassium iodide solution.

Statistics. All statistical analysis was performed using Graphpad Prism software. Quantitative results for in vitro experiments were presented as mean ± SEM. Statistical analyses were performed by the *t*-test or analysis of variance (ANOVA) tests followed by post-test multiple comparison as described in the figure captions. P values of less than 0.05 were considered significant.

RESULTS

Design of the miRNA-Inducible Conditional ASO. The miRNA-triggered conditional ASO is a duplex (double-stranded oligonucleotides) formed by an extended ASO strand and a locking strand (Figure 1a). The extended ASO strand was comprised of two domains: the parental ASO and a partial miRNA sequence attached to the 5′ terminus of the parental ASO. We termed this strand the partial miRNA-ASO (pM-ASO) strand. The partial miRNA domain lacks the key seeding sequences (2−8 nt) of the miRNA. Since the seeding sequence of miRNA by itself could knockdown its target genes,[33] it was not included to prevent the potential unintentional effect. The locking strand is composed of the complementary sequence to the full mature miRNA and the parental ASO. We

https://doi.org/10.1021/acschembio.1c00387
ACS Chem. Biol. XXXX, XXX, XXX−XXX

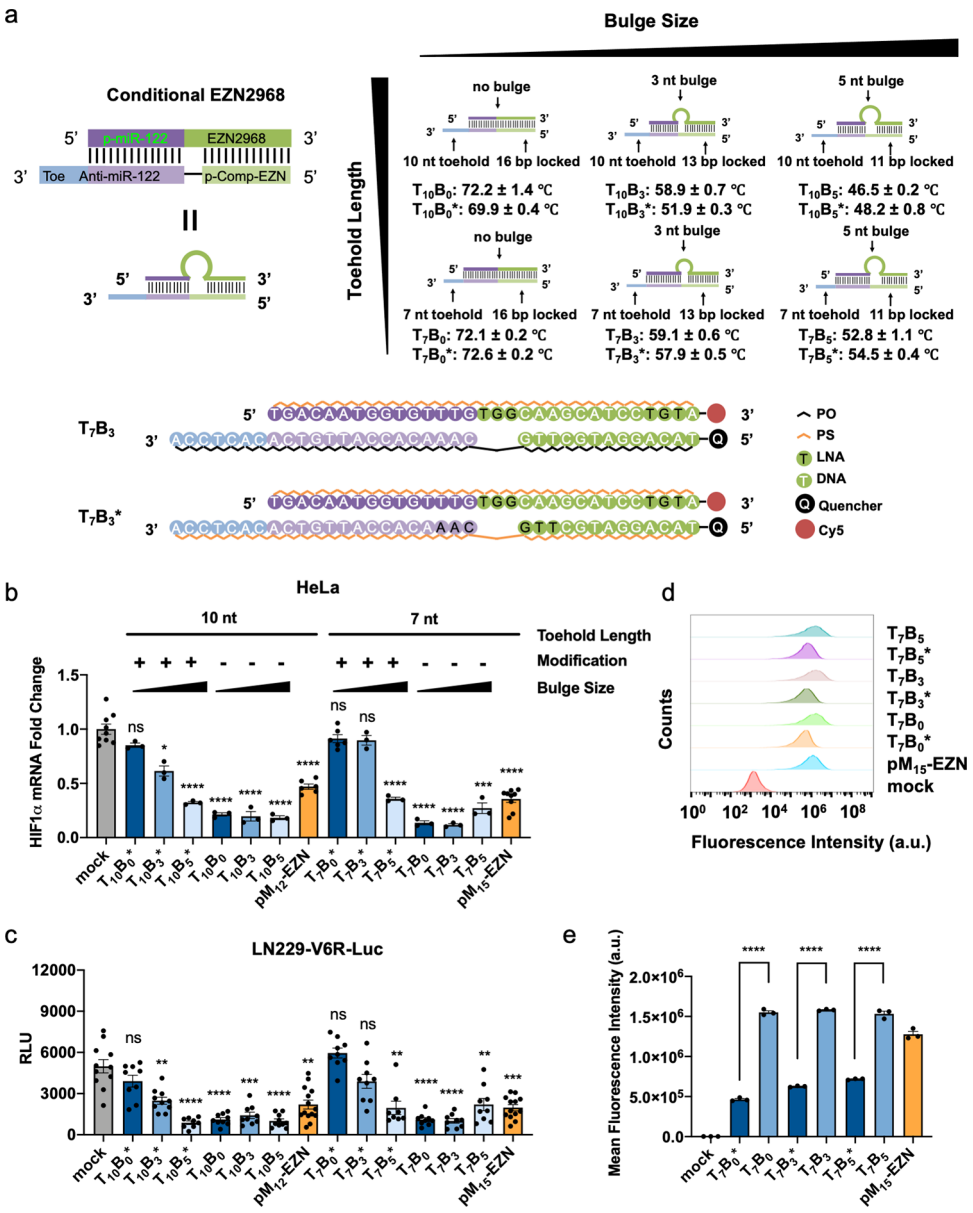

Figure 4. Screening for conditional EZN2968 with minimum spontaneous activation. (a) Structure and chemistry of conditional EZN2968. Conditional EZN2968 is composed of a pM-EZN strand and a locking strand. By tuning the length of the two strands, the duplexes with different toehold lengths and bulge sizes were created. Chemically modified (annotated with "*") and unmodified locking strands were also compared to assess the role of nucleases in competence of the locking strand to inhibit EZN2968 activity. Sequences of T_7B_3 and T_7B_3* are shown as examples. (b) HeLa cells were transfected with 10 nM concentration of each duplex and incubated for 24 h. HIF1α mRNA levels were quantified by qPCR normalized to 18S. The error bars represent SEM. ** $p < 0.01$, *** $p < 0.001$, and **** $p < 0.0001$; Brown−Forsythe and Welch ANOVA tests with Dunnett's T3 multiple comparison. (c) LN229-V6R-Luc cells transfected with 10 nM concentration of each duplex for 4 h were treated with 20 μM IOX4 for another 20 h before the luciferase assay was conducted to assess HIF1α activity. The error bars represent SEM. ** $p < 0.01$, *** $p < 0.001$, and **** $p < 0.0001$; Brown−Forsythe and Welch ANOVA tests with Dunnett's T3 multiple comparison. (d, e) (d) Histogram and (e) mean fluorescence intensity of HeLa cells transfected with 10 nM Cy5/quencher labeled duplexes and incubated for 24 h, quantified by flow cytometry. The error bars represent SEM. ** $p < 0.01$, *** $p < 0.001$, and **** $p < 0.0001$; one-way ANOVA with Tukey's multiple comparison.

hypothesized that the conditional ASO duplex is kept inactive since the ASO is hybridized to the locking strand in the absence of the miRNA trigger. When the miRNA trigger is present, however, it binds to the toehold domain of the locking strand, initiating a competition reaction between the miRNA and pM-ASO strand for binding to the locking strand. If the binding of miRNA to the locking strand is favorable, which can be achieved by partial hybridization of the ASO domain to the locking strand to reduce the stability of the duplex after miR-122 binding, the pM-ASO is displaced, exposing and activating the ASO sequence. The activated ASO can then bind to the target mRNA and recruit RNase H to cleave it (Figure 1a). In the case of the miR-122-inducible HIF1α ASO, the parental HIF1α ASO for the conditional ASO is EZN2968,[25] which is a 16 nt oligonucleotide with a phosphorothioate (PS) backbone and LNA modification. The miR-122-inducible HIF1α ASO is a duplex formed by the pM-EZN strand and the locking strand.

To create the most selective and efficient miR-122-inducible EZN2968 ASO, we optimized for (1) minimum spontaneous dissociation (leakage) of the duplex in the absence of miR-122

https://doi.org/10.1021/acschembio.1c00387
ACS Chem. Biol. XXXX, XXX, XXX−XXX

to keep the HIF1α ASO activity low in basal conditions and (2) a high miR-122 sensitivity that leads to maximum activation of the HIF1α ASO. These criteria can be met when the free energy (ΔG) of the conditional EZN2968 duplex is lower than the ΔG of pM-EZN/HIF1α mRNA duplex and higher than the ΔG of the miR-122/locking strand duplex, as shown in Figure 1b and Figure S1a. The displacement mediated by the toehold (α domain) on the locking strand reduces the kinetic barrier for miR-122-triggered activation. We predicted that due to the thermostability of the completely locked duplex, its miR-122 sensitivity would be limited. To rationally enhance sensitivity to miR-122, several nucleotides could be removed (length of the β or γ domain) from the complementary sequence of EZN2968 to render the duplex either in an end-destabilized conformation or in a bulge-destabilized conformation (Figure 2a). The single-stranded β or γ domain in the pM-EZN strand may also function as a toehold and drive the dehybridization of conditional EZN2968 upon binding of HIF1α mRNA and reduce the kinetic barrier for HIF1α mRNA-triggered leakage activation (Figure 1b and Figure S1a). Therefore, fine tuning and optimization of the duplex conformation and length of each domain was required.

We hypothesized that bulge destabilization is advantageous over end destabilization in terms of lowering leakage activation triggered by HIF1α mRNA due to the relative inaccessibility of the bulge region (γ domain) for mRNA binding.[34,35] To test this hypothesis, we created a library of chemically unmodified duplexes with different lengths (4, 7, and 10 nt) of the toehold (α domain) and numbers of nucleotides removed in the duplex region (length of the β or γ domain) for both conformations. The duplexes were labeled with Cy5 on the 3′ termini of the pM-EZN strand and a quencher on the 5′ termini of the locking strand. Their dehybridization upon triggering by an HIF1α mRNA mimicking strand was quantified by measuring the increase in fluorescence intensity driven by dequenched Cy5 (Figure 2b). The results showed that the percentage of displaced pM-EZN for all bulge-destabilized duplexes was lower than that for their end-destabilized counterparts, except for the ones with a 7 nt bulge and 7 or 10 nt toehold (Figure 2d). The low stability of 7 nt bulge duplexes may be attributed to a lower thermodynamic stability because of the shorter double-stranded domains and the lower stability of duplexes with larger bulge sizes (Figure S1b). miRNA-triggered activation was also measured with a similar assay, where the Cy5/quencher-labeled duplexes were incubated with an miR-122 mimicking sequence (Figure 2c). The results showed that the miRNA-triggered activation increased as the length of the β or γ domain was increased (Figure 2e), due to the reduced stability of the duplexes indicated by calculated ΔG (Figure S1b). In general, the bulge-destabilized duplex conformation resulted in a higher ratio of miR-122-triggered displacement to mRNA-triggered displacement (Figure 2f). Based on these results, we decided to use the bulge-destabilized duplex conformation for the in vitro screen. It should be noted that in the bulge destabilized design, it is possible that an intermediate consisting of pM-EZN/locking strand/miR-122 may form. After mRNA binds to the linearized γ domain and displaces the locking strand from pM-EZN, the locking strand/miRNA duplex (or the "waste" in Figure 1a) would be released.

pM-EZN Strands Knock Down HIF1α in a Dose- and Time-Dependent Manner. To evaluate the effect of the partial miR-122 sequence on pM-EZN strands for HIF1α knockdown, we created pM-EZN with 12 nt (pM_{12}-EZN) or 15 nt (pM_{15}-EZN) extension on the 5′ termini of EZN2968 (Figure 3a). The pM-EZN strands maintained the LNA modification and the PS backbone as the parental EZN2968. We transfected pM_{12}-EZN or pM_{15}-EZN in U373 cells, a glioblastoma cell line that expresses high levels of HIF1α and negligible levels of miR-122 (Figure S2). We found that these two strands knocked down HIF1α mRNA and protein in a dose- and time-dependent manner (Figure 3b−d). We further tested pM_{12}-EZN or pM_{15}-EZN in LN229-V6R-Luc cells, an HIF1α reporter cell line (Figure 3e).[36] IOX4, a prolyl-hydroxylase 2 (PHD2) inhibitor,[37] was used to induce luciferase expression. Consistent with mRNA knockdown in U373 cells, transfection of 10 nM pM_{12}-EZN and pM_{15}-EZN led to significant reduction of luciferase expression in this cell line (Figure 3e).

Screening for Conditional EZN2968 with Minimum Spontaneous Leakage In Vitro. To investigate the effect of chemical modification, bulge size, and toehold length on the efficacy of locking strands in terms of spontaneous leakage of HIF1α knockdown activity, we created a library of 12 conditional EZN2968s by annealing pM_{12}-EZN or pM_{15}-EZN with six different locking strands (B_0, B_3, B_5, B_0*, B_3*, and B_5*) at a 1:1 ratio in PBS. The locking strands are named based on the size of the bulge when hybridized to the pM-EZN strand and the chemical modification. For example, B_0 is the unmodified locking strand that does not generate a bulge when hybridized to pM-EZN strands; whereas B_3* represents the modified locking strand forming a 3 nt bulge duplex when hybridized to pM-EZN strands. Because PS modification reduces affinity for the complementary nucleic acid by ∼0.5 °C per incorporation,[38] LNA modifications were also incorporated in the locking strands to compensate for and maintain the thermodynamic stability of the duplex, so that it displays a similar melting temperature (T_m) compared to its unmodified counterpart (Figure 4a). The resulting duplex library included permutations with a bulge size of 0, 3, or 5 nt, a toehold length of 7 or 10 nt, and chemically modified (PS/LNA) or unmodified locking strands (Figure 4a). The duplexes are termed based on the toehold length and bulge size of the duplex. For example, the duplex formed by pM_{12}-EZN and B_3* has a 7 nt toehold and a 3 nt bulge; therefore, it is named T_7B_3*.

Transfection experiments in HeLa cells showed that PS/LNA chemical modification of the locking strand was critical for maintaining the ASO in the inactive state. We performed these experiments in HeLa cells because they do not express a measurable level of miR-122 (Figure S2). We found that all the unmodified locking strands B_0, B_3, and B_5 failed to inhibit ASO activity as measured by RT-qPCR and using the luciferase reporter cell line (Figure 4b,c). Importantly, incorporating locking strands with the PS and LNA modifications showed substantial improvement, resulting in dampened knockdown of HIF1α (Figure 4b,c). Given that the T_m values of B_0 and B_0* against the pM-EZN strands are similar, this indicates that the differential response is not driven by the thermodynamic difference between the conventional nucleobases and the PS/LNA nucleic acids. The failure in locking efficacy by unmodified locking strands may be due to their nuclease susceptibility, which leads to degradation of the locking strands and the spontaneous activation of the pM-EZN. A similar observation was reported by Nishina et al. that hybridization of

https://doi.org/10.1021/acschembio.1c00387
ACS Chem. Biol. XXXX, XXX, XXX−XXX

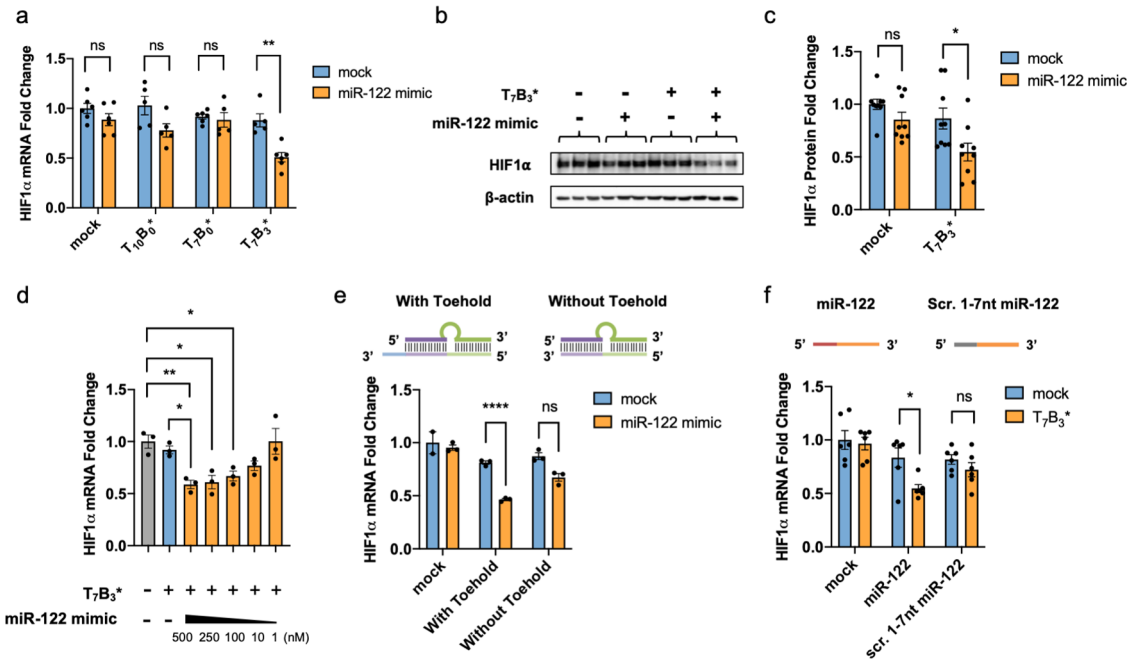

Figure 5. Activation of conditional EZN2968 triggered by the miR-122 mimic. (a–c) U373 cells were cotransfected with 10 nM $T_{10}B_0$*, T_7B_0*, or T_7B_3* and 500 nM miR-122 mimic. After 24 h, (a) HIF1α mRNA levels were quantified by qPCR and normalized to 18S, while (b,c) HIF1α protein was quantified by the Western Blot. * $p < 0.05$, *t*-test. (d) U373 cells were cotransfected with 10 nM T_7B_3* and different concentrations of the miR-122 mimic. After 24 h, HIF1α mRNA levels were quantified by qPCR and normalized to 18S. The error bars represent SEM. * $p < 0.05$; ** $p < 0.01$; one-way ANOVA with Tukey's multiple comparison. (e, f) U373 cells were cotransfected with (e) 10 nM T_7B_3* with or without a toehold and 500 nM miR-122 mimic or (f) 10 nM T_7B_3* and 100 nM miR-122 mimic or scr. 1–7 nt miR-122. After 24 h, HIF1α mRNA levels were quantified by qPCR and normalized to 18S. The error bars represent SEM. * $p < 0.05$; **** $p < 0.0001$; *t*-test.

a partially modified RNA strand to an ASO did not inhibit its gene silencing efficacy due to degradation of the RNA strand.[39] Because the PS/LNA locking strands (B_0*, B_3*, and B_5*) are fully modified and share the same chemical modification with the ASO itself, activation of the ASO due to degradation of only the locking strand is unlikely. To test this prediction, we transfected HeLa cells with pM_{15}-EZN duplexes labeled with the Cy5 and quencher pair and measured the cell-associated fluorescence by flow cytometry (Figure 4d,e). As expected, cells transfected with pM_{15}-EZN duplexes with unmodified locking strands (T_7B_0, T_7B_3, and T_7B_5) resulted in similar and even slightly higher levels of fluorescence intensity compared to cells transfected with the single-stranded pM_{15}-EZN alone, indicating complete dissociation of the locking strand and pM_{15}-EZN strand (Figure 4d,e). The slightly higher level of fluorescence intensity was consistent with the higher HIF1α knockdown efficacy by the duplexes with unmodified locking strands compared to the pM_{15}-EZN-only group (Figure 4b,c). This may be due to the higher transfection efficiency of double-stranded DNA labeled with both Cy5 and the quencher (hydrophobic moieties) compared to single-stranded DNA labeled with only Cy5 in HeLa cells.[40] In contrast, pM_{15}-EZN duplexes with modified locking strands (T_7B_0*, T_7B_3*, and T_7B_5*) resulted in reduced fluorescence intensity compared to the pM_{15}-EZN-only group, showing that the duplexes remain primarily locked (hybridized) 24 h after transfection.

We also found that increasing the bulge size decreased the thermodynamic stability of the duplex (Figure 4a) while increasing the level of spontaneous activation of the conditional ASO (Figure 4b,c). T_7B_3* did not knockdown HIF1α, whereas $T_{10}B_3$* knocked down HIF1α significantly, indicating that the length of the toehold and branch migration domain also plays an important role in the spontaneous leakage. The conclusions that chemical modification of the locking strand and stable binding to the ASO (T_m > 58 °C) are two necessary requirements to inhibit EZN2968 were further validated in U373 cells, lacking endogenous miR-122 expression, by both RT-qPCR and Western Blot analysis (Figure S3). Based on these results, we chose to move forward using the $T_{10}B_0$*, T_7B_0*, and T_7B_3* duplexes, with low spontaneous activation, to test miR-122-induced HIF1α knockdown.

Synthetic miR-122 Mimic Triggers Activation of Conditional EZN2968 In Vitro. Next, we tested if conditional EZN2968 could be activated in vitro by using an exogenously transfected miR-122 mimic in U373 cells. To minimize the complexity of the experiment and ASO activation prior to its entry to the cells, we prepared the transfection mixture of the conditional EZN2968 duplex ($T_{10}B_0$*, T_7B_0*, or T_7B_3*) and miR-122 mimic separately with Oligofectamine and added the two solutions to the cells simultaneously. We found that the displacement reaction in the transfection mixture was inhibited (Figure S4). After 24 h incubation post-transfection, 10 nM T_7B_3* alone did not show significant downregulation of HIF1α mRNA, whereas 10 nM T_7B_3* cotransfected with the 500 nM miR-122 mimic downregulated HIF1α mRNA by ~50% (Figure 5a). In contrast, $T_{10}B_0$* and T_7B_0*, which have no bulge, did not knockdown HIF1α mRNA when cotransfected with miR-122 mimic (Figure 5a). These results confirmed our initial hypothesis that completely locked duplexes without a bulge exhibit low miR-122 sensitivity, and destabilization of the duplex is necessary for enhancing miR-122 sensitivity. Cotransfection of T_7B_3* and the miR-122 mimic also downregulated HIF1α protein levels in U373 cells after 24 h incubation (Figure 5b,c).

https://doi.org/10.1021/acschembio.1c00387
ACS Chem. Biol. XXXX, XXX, XXX–XXX

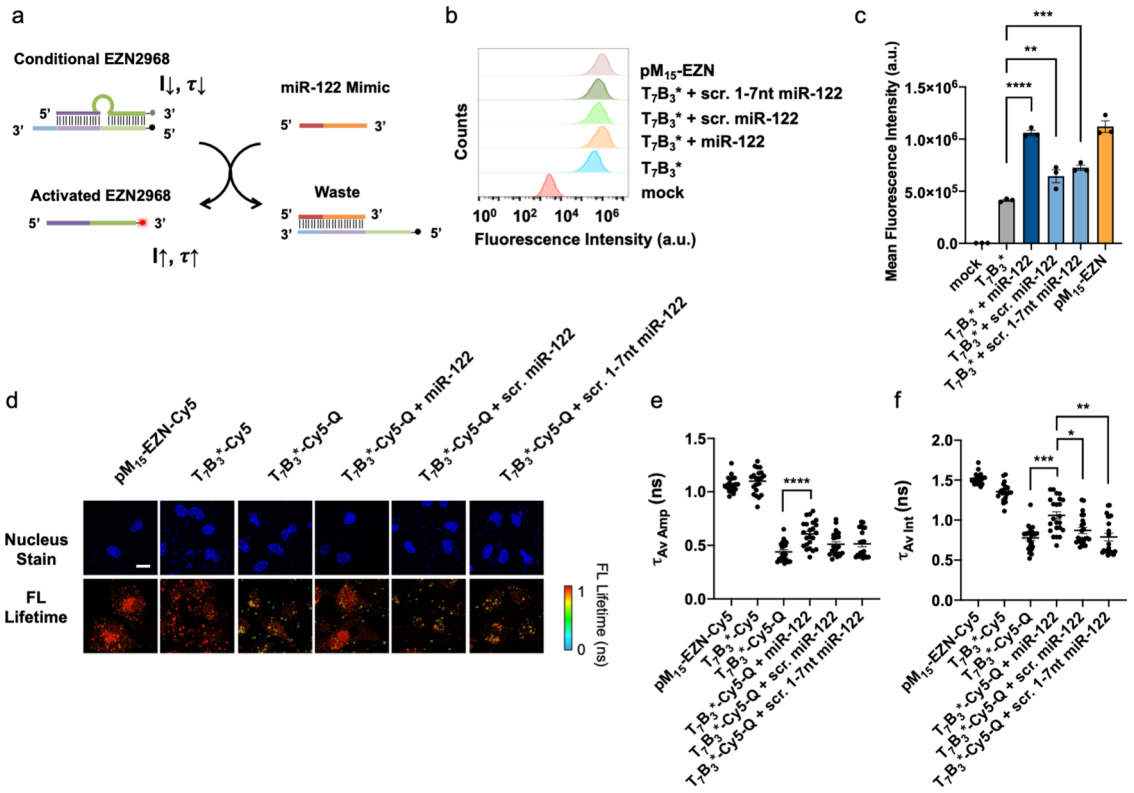

Figure 6. Flow cytometry and fluorescence lifetime imaging (FLIM) to evaluate the specificity of T_7B_3* to the miR-122 mimic. (a) Scheme showing fluorescence dequenching and fluorescence lifetime increases of Cy5 due to activation of T_7B_3* by the miR-122 mimic. (b) Histogram and (c) mean fluorescence intensity of U373 cells cotransfected with 10 nM Cy5/quencher-labeled T_7B_3* and 500 nM miR-122, scr. miR-122, and scr. 1−7 nt miR-122 and incubated for 24 h. The error bars represent SEM. ** $p < 0.01$, *** $p < 0.001$, and **** $p < 0.0001$; one-way ANOVA with Tukey's multiple comparison. (d) Representative fluorescence lifetime images (scale bar = 20 μm), (e) amplitude-averaged, and (f) intensity-averaged fluorescence lifetime of U373 cells transfected with 10 nM Cy5/quencher-labeled T_7B_3* and 500 nM miR-122, scr. miR-122, or scr. 1−7 nt miR-122 and incubated for 24 h. Cy5-labeled pM_{15}-EZN or Cy5-labeled T_7B_3* transfected cells were positive controls, and Cy5/quencher-labeled T_7B_3* transfected cells were negative controls. Each data point represents the calculated fluorescence lifetime of one image. The error bars represent SEM. * $p < 0.05$, ** $p < 0.01$, *** $p < 0.001$, and **** $p < 0.0001$; Brown−Forsythe and Welch ANOVA tests with Dunnett's T3 multiple comparison.

Given the miR-122 sensitivity of T_7B_3*, we next quantified its concentration-dependent response to miR-122. We found that HIF1α mRNA levels decreased with increasing miR-122 concentrations in a concentration-dependent manner (Figure 5d). Although we tested miR-122 concentrations of 1−500 nM, only when the miR-122 mimic concentration was above 100 nM did T_7B_3* show significant knockdown of HIF1α (Figure 5d). In order to validate that ASO activation is driven through toehold-mediated strand displacement, we created a T_7B_3* with its toehold domain truncated. After cotransfection with the miR-122 mimic, T_7B_3* lacking the toehold showed a dampened and not statistically significant knockdown of HIF1α mRNA, in contrast to T_7B_3* with the toehold (Figure 5e). This knockdown is likely caused by displacement that is not mediated by the toehold over the 24 h duration of the experiment. In addition, we cotransfected T_7B_3* with the miR-122 mimic or an miR-122 sequence with a scrambled (scr.) toehold-binding domain (1−7 nt from 5′ end) and found that the scr. 1−7 nt miR-122 did not trigger significant HIF1α knockdown (Figure 5f). These results demonstrate that toehold binding of miR-122 facilitates the activation of the conditional EZN2968, both thermodynamically (because of a weaker binding between the scr. 1−7 nt miR-122 and locking strand) and kinetically (through acceleration of the displacement reaction).

Activation of Conditional EZN2968 Is Specific to miR-122. To test the specificity of conditional EZN2968 activation in response to the miR-122 sequence, we used two scrambled miR-122 sequences: one that is completely scrambled (scr. miR-122) and the other with the scrambled toehold binding domain at 1−7 nt of miR-122 (scr. 1−7 nt miR-122). Activation kinetics of T_7B_3* incubated with each miRNA sequence in buffer showed the highest activation rate for the miR-122 mimic group followed by the scr. 1−7 nt miR-122 group. T_7B_3* incubated with scr. miR-122 showed very slow activation, probably due to nonspecific interaction (Figure S5). Each miRNA sequence was cotransfected with conditional ASO T_7B_3* in U373 cells. The T_7B_3* duplex was dual labeled with a Cy5 at the 3′ end of the pM_{15}-EZN strand and a quencher on the 5′ end of the B_3* strand (Figure 6a). These fluorescence labels generated a turn-on fluorescence response upon dehybridization of the conditional ASO and provided a readout of displacement. After 24 h incubation with the miR-122 mimic (500 nM) along with T_7B_3* (10 nM), the cell-associated fluorescence showed the greatest increase compared to the T_7B_3*-only transfected cells. In contrast, U373 cells cotransfected with T_7B_3* and scr. miR-122 or scr. 1−7 nt miR-122 showed a weaker fluorescence (Figure 6b,c). Indeed, the cells cotransfected with T_7B_3*, and miR-122 showed fluorescence levels on par with those of the Cy-5-tagged

https://doi.org/10.1021/acschembio.1c00387
ACS Chem. Biol. XXXX, XXX, XXX−XXX

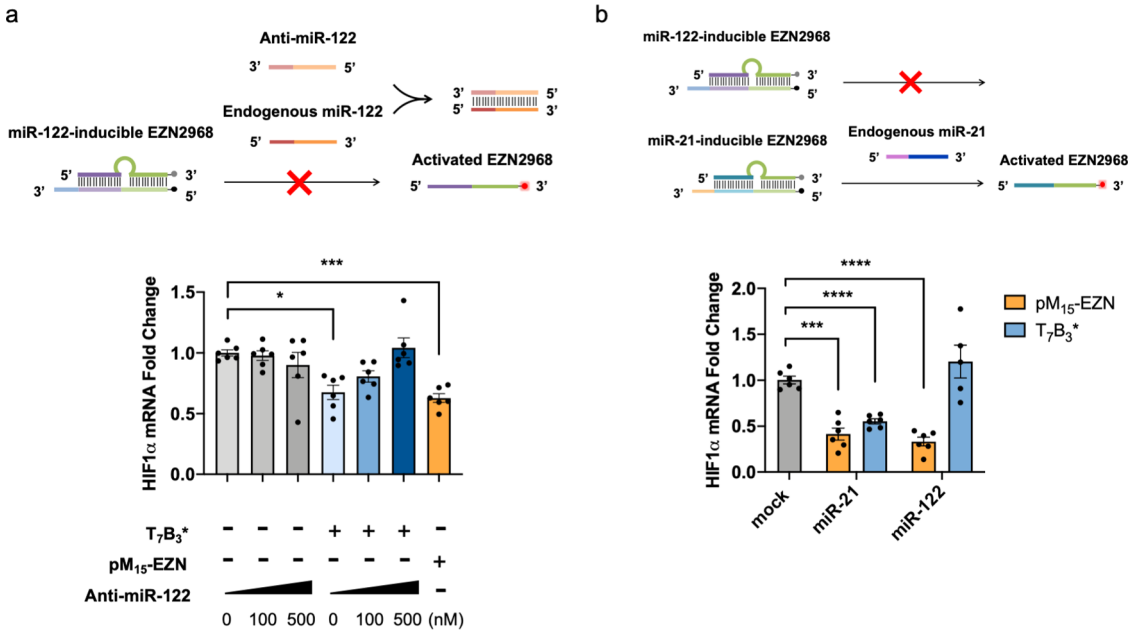

Figure 7. HIF1α knockdown induced by endogenous miRNAs. (a) Huh7 cells were transfected with different concentrations of anti-miR-122 and 50 nM T_7B_3* sequentially with a 6 h interval. After 24 h, HIF1α mRNA levels were quantified by qPCR and normalized to 18 s. The error bars represent SEM. * $p < 0.05$; *** $p < 0.001$; Brown−Forsythe and Welch ANOVA tests with Dunnett's T3 multiple comparison. (b) U373 cells were transfected with 10 nM miR-122- or miR-21-inducible T_7B_3* for 24 h. Corresponding pM_{15}-EZN strands were transfected as positive controls. HIF1α mRNA levels were quantified by qPCR and normalized to 18S. The error bars represent SEM. *** $p < 0.001$; **** $p < 0.0001$; Brown−Forsythe and Welch ANOVA tests with Dunnett's T3 multiple comparison.

pM_{15}-EZN, which confirms miR-122-driven unlocking of the conditional ASO. The release of the ASO in the presence of the scrambled miR-122 mimic is likely due to nonspecific interaction between the ASO duplex and the mimic.

To further validate the fluorescence intensity-based assay, we also measured the fluorescence lifetime of the Cy5/quencher-tagged T_7B_3*, confirming the specificity of miRNA-inducible ASO activation (Figure 6a). Fluorescence lifetime measurements provide a concentration-independent readout of the fluorophore local environment.[41] In PBS, Cy5-labeled pM_{15}-EZN strands (pM_{15}-EZN-Cy5) showed an amplitude-averaged lifetime ($\tau_{AV\ Amp}$) of 1.7 ns and an intensity-averaged lifetime ($\tau_{AV\ Int}$) of 1.9 ns, whereas after hybridizing the pM_{15}-EZN strand with locking strand B_3* tagged with the quencher (T_7B_3*-Cy5-Q), $\tau_{AV\ Amp}$ and $\tau_{AV\ Int}$ of Cy5 decreased to 0.4 and 0.7 ns, respectively (Figure S5). After incubation of 10 nM T_7B_3*-Cy5-Q with the 500 nM miR-122 mimic, $\tau_{AV\ Amp}$ and $\tau_{AV\ Int}$ increased to 0.9 and 1.5 ns (Figure S5). However, the fluorescence lifetime of T_7B_3*-Cy5-Q with scr. miR-122 and scr. 1−7 nt miR-122 showed only a slight increase compared to the T_7B_3*-Cy5-Q-only group, which is likely due to nonspecific binding of the miRNA mimic to T_7B_3* (Figure S6). Next, we cotransfected U373 cells with T_7B_3*-Cy5-Q and the miR-122 mimic or scrambled miRNA triggers. After 24 h, FLIM was conducted on the cells to measure Cy5 fluorescence lifetime within cells. pM_{15}-EZN-Cy5 and T_7B_3* labeled with only Cy5 but not the quencher (T_7B_3*-Cy5) were also transfected as positive controls. As shown in Figure 6d−f, cells cotransfected with T_7B_3*-Cy5-Q and miR-122 mimics showed a significant increase of Cy5 fluorescence lifetime compared to the T_7B_3*-Cy5-Q-only group, whereas cells cotransfected with T_7B_3*-Cy5-Q and scr. miR-122 or scr. 1−7 nt miR-122 did not show a significant increase in fluorescence lifetime. Together, these results confirm that dequenching of Cy5 is caused by dehybridization of the pM_{15}-EZN and locking strand B_3*, and this response is specifically triggered by miR-122 and mediated by the toehold domain.

Endogenous miR-122 Induces HIF1α Knockdown by Conditional EZN2968. We next tested whether endogenous miR-122 could induce HIF1α knockdown by T_7B_3* and if the activation can be inhibited by reducing endogenous miR-122 levels in a hepatocyte cell line, Huh7 cell. This cell line naturally expresses high levels of miR-122 (Figure S3). We treated Huh7 cells with different concentrations of anti-miR-122 to reduce miR-122 levels (Figure S7) and then transfected with T_7B_3*. T_7B_3* knocked down HIF1α to a similar level compared to the pM_{15}-EZN-only group, indicating its activation. In addition, anti-miR-122 inhibited the HIF1α knockdown efficacy of T_7B_3* in a concentration-dependent manner (Figure 7a). Together, these data show that the conditional EZN2968 activity is induced by endogenous miR-122 and depends on miR-122 expression levels in the cells.

In principle, the conditional EZN2968 design is modular, and one could engineer responses to virtually any miRNA trigger. To test the modular design concept, we created an miR-21-inducible EZN2968 with the same toehold length and bulge size as miR-122-inducible T_7B_3* (Table S3). This new duplex was transfected into U373 cells, which express high levels of miR-21 (Figure S8). miR-21-inducible T_7B_3* showed a significant knockdown of HIF1α, while the miR-122-inducible T_7B_3* did not (Figure 7b). Thus, by simply changing the miRNA sequence in the extended EZN2968 ASO and the miRNA-complementary sequence in the locking strand, it was possible to generate another conditional EZN2968 ASO triggered by endogenous miR-21. Flow cytometry further showed that cells transfected with Cy5/quencher-labeled miR-21-inducible duplex showed a slightly higher fluorescence compared to the miR-122-inducible counterpart, suggesting

https://doi.org/10.1021/acschembio.1c00387
ACS Chem. Biol. XXXX, XXX, XXX−XXX

displacement of the duplex triggered by miR-21 (Figure S9). The small differences in fluorescence intensity between miR-21 and miR-122-inducible duplexes may suggest that the downregulation of HIF1α by the miR-21-inducible ASO is caused by a small fraction of ASOs that are activated. These results demonstrate the concept of the miRNA-inducible, modular conditional ASO therapeutics, which can be rapidly designed and synthesized based on the disease- or cell-specific miRNAs.

DISCUSSION

In this study, we established design principles and experimental approaches for harnessing dynamic strand displacement reactions for the purpose of generating conditional ASO therapeutics. We used miR-122-triggered activation of the EZN2968 ASO as a model and systemically explored how the interplay of the molecular structure, nucleic acid chemistry, and thermostability determine the performance of the conditional ASO in cells. We showed that EZN2968-mediated HIF1α knockdown was triggered by either a synthetic miR-122 mimic or endogenously expressed miR-122 using anti-miR-122. Together, this proof-of-concept study demonstrates the applicability of conditional ASOs in a cell-type specific manner.

Most ASOs are 16 nts long, while most miRNAs are 22 nt, and accordingly, our design is not specific to HIF1α and miR-122. In principle, conditional ASOs can be engineered to trigger inhibition of any mRNA using other specific miRNA triggers. This concept was further supported by adapting the conditional EZN2968 ASO design to miR-21, showing that miR-21-inducible EZN2968 knocked down HIF1α in cells expressing high levels of miR-21. This miR-21-inducible HIF1α inhibitor could be a potential therapeutic for cancer, given the high expression level and significant roles of miR-21[42] and HIF1α in cancer development. The main advantage of this design is the enhancement in specificity: allowing therapeutic oligonucleotides to exclusively downregulate gene expression transiently in a cell-type specific manner. Conditional ASOs will be most desirable when target mRNAs are broadly expressed across many cell types but where selective inhibition would be desirable. HIF1α is a good example, as it plays essential roles in a wide variety of normal and pathological cellular processes. In addition to miRNAs, other cellular RNAs can also be used to trigger the conditional ASOs. In our study, we used miRNA as a trigger because its expression is highly regulated in certain cell types and disease conditions and because of its innate functions in binding to complementary nucleic acids. While our work here was performed using transfection reagents, conditional oligonucleotides can be delivered with other commonly used delivery methods, such as lipid conjugation, spherical nucleic acids, and other nanomaterial delivery vehicles, to facilitate cellular internalization.

As for future directions, optimization of conditional ASOs can be performed to identify designs that offer a wider dynamic range, higher miRNA sensitivity, and faster activation kinetics, possibly through modulation of chemical modifications on different domains of the duplex. In addition, because dehybridization may occur for double-stranded conditional ASOs due to gradual dilution, bridging the 3′ terminus of the pM-ASO strand and the 5′ end of the locking strand could potentially reduce spontaneous activation and provide reversibility of the conditional ASOs.

Since systemically delivered oligonucleotides tend to accumulate in the liver,[43] conditionally silencing oligonucleotide activity in the liver could be beneficial. This "on-to-off" switching mechanism could potentially be achieved through extending both termini of the ASO with partial miR-122 complementary sequences, which allows formation of three-way junctions to conceal the ASO sequence. Because additional sequences are inserted or extended in the conditional ASO therapeutics, rational design and optimization is needed to prevent the formation of stable secondary structures, which might eliminate their RNA binding ability. In addition, off-target effects caused by extended or inserted sequences need to be evaluated through transcriptomic studies to validate the safety of each conditional ASO therapeutic. The conditional ASOs with miRNA triggers could improve the safety of these therapeutics through cell-type specific activation.

ASSOCIATED CONTENT

Supporting Information

The Supporting Information is available free of charge at https://pubs.acs.org/doi/10.1021/acschembio.1c00387.

NUPACK calculation of free energy of conditional EZN2968, miRNA expression levels, activation kinetics of conditional ENZ2968 in buffer, fluorescence lifetime measurement in buffer, and oligonucleotide and primer sequences (PDF)

AUTHOR INFORMATION

Corresponding Authors

Khalid Salaita − *Wallace H. Coulter Department of Biomedical Engineering, Emory University and Georgia Institute of Technology, Atlanta, Georgia 30332, United States; Department of Chemistry, Emory University, Atlanta, Georgia 30322, United States;* orcid.org/0000-0003-4138-3477; Email: k.salaita@emory.edu

Hanjoong Jo − *Wallace H. Coulter Department of Biomedical Engineering, Emory University and Georgia Institute of Technology, Atlanta, Georgia 30332, United States; Division of Cardiology, Department of Medicine, Emory University, Atlanta, Georgia 30322, United States;* orcid.org/0000-0003-1833-372X; Email: hjo@emory.edu

Authors

Jiahui Zhang − *Wallace H. Coulter Department of Biomedical Engineering, Emory University and Georgia Institute of Technology, Atlanta, Georgia 30332, United States;* orcid.org/0000-0002-4949-6217

Radhika Sharma − *Department of Chemistry, Emory University, Atlanta, Georgia 30322, United States*

Kitae Ryu − *Wallace H. Coulter Department of Biomedical Engineering, Emory University and Georgia Institute of Technology, Atlanta, Georgia 30332, United States*

Patrick Shen − *Department of Chemistry, Emory University, Atlanta, Georgia 30322, United States*

Complete contact information is available at: https://pubs.acs.org/10.1021/acschembio.1c00387

Funding

This work was supported in part by funding from National Institutes of Health grants R01HL142866 to K.S. and HL119798 and HL095070 to H.J.

Notes

The authors declare no competing financial interest.

■ ACKNOWLEDGMENTS

We would like to thank E. van Meir's Lab at O'Neal Comprehensive Cancer Center, University of Alabama, Birmingham, for providing LN229-V6R-Luc cells and A. Grakoui's Lab at Emory University for providing Huh7 cells.

■ REFERENCES

(1) Walder, R. Y.; Walder, J. A. Role of RNase H in hybrid-arrested translation by antisense oligonucleotides. *Proc. Natl. Acad. Sci. U. S. A.* **1988**, *85*, 5011−5015.
(2) Bennett, C. F. Therapeutic antisense oligonucleotides are coming of age. *Annu. Rev. Med.* **2019**, *70*, 307−321.
(3) Bennett, C. F.; Baker, B. F.; Pham, N.; Swayze, E.; Geary, R. S. Pharmacology of antisense drugs. *Annu. Rev. Pharmacol. Toxicol.* **2017**, *57*, 81−105.
(4) Kim, J.; Hu, C.; Moufawad el Achkar, C.; Black, L. E.; Douville, J.; Larson, A.; Pendergast, M. K.; Goldkind, S. F.; Lee, E. A.; Kuniholm, A.; Soucy, A.; Vaze, J.; Belur, N. R.; Fredriksen, K.; Stojkovska, I.; Tsytsykova, A.; Armant, M.; DiDonato, R. L.; Choi, J.; Cornelissen, L.; Pereira, L. M.; Augustine, E. F.; Genetti, C. A.; Dies, K.; Barton, B.; Williams, L.; Goodlett, B. D.; Riley, B. L.; Pasternak, A.; Berry, E. R.; Pflock, K. A.; Chu, S.; Reed, C.; Tyndall, K.; Agrawal, P. B.; Beggs, A. H.; Grant, P. E.; Urion, D. K.; Snyder, R. O.; Waisbren, S. E.; Poduri, A.; Park, P. J.; Patterson, A.; Biffi, A.; Mazzulli, J. R.; Bodamer, O.; Berde, C. B.; Yu, T. W. Patient-customized oligonucleotide therapy for a rare genetic disease. *N. Engl. J. Med.* **2019**, *381*, 1644−1652.
(5) Khvorova, A.; Watts, J. K. The chemical evolution of oligonucleotide therapies of clinical utility. *Nat. Biotechnol.* **2017**, *35*, 238.
(6) Craig, K.; Abrams, M.; Amiji, M. Recent preclinical and clinical advances in oligonucleotide conjugates. *Expert Opin. Drug Deliv.* **2018**, *15*, 629−640.
(7) Sazani, P.; Gemignani, F.; Kang, S.-H.; Maier, M. A.; Manoharan, M.; Persmark, M.; Bortner, D.; Kole, R. Systemically delivered antisense oligomers upregulate gene expression in mouse tissues. *Nat. Biotechnol.* **2002**, *20*, 1228−1233.
(8) Osborn, M. F.; Khvorova, A. Improving siRNA delivery in vivo through lipid conjugation. *Nucleic Acid Ther.* **2018**, *28*, 128−136.
(9) Rigo, F.; Chun, S. J.; Norris, D. A.; Hung, G.; Lee, S.; Matson, J.; Fey, R. A.; Gaus, H.; Hua, Y.; Grundy, J. S.; Krainer, A. R.; Henry, S. P.; Bennett, C. F. Pharmacology of a central nervous system delivered 2′-O-methoxyethyl−modified survival of motor neuron splicing oligonucleotide in mice and nonhuman primates. *J. Pharmacol. Exp. Ther.* **2014**, *350*, 46−55.
(10) Young, D. D.; Lively, M. O.; Deiters, A. Activation and deactivation of DNAzyme and antisense function with light for the photochemical regulation of gene expression in mammalian cells. *J. Am. Chem. Soc.* **2010**, *132*, 6183−6193.
(11) Deiters, A.; Garner, R. A.; Lusic, H.; Govan, J. M.; Dush, M.; Nascone-Yoder, N. M.; Yoder, J. A. Photocaged morpholino oligomers for the light-regulation of gene function in zebrafish and Xenopus embryos. *J. Am. Chem. Soc.* **2010**, *132*, 15644−15650.
(12) Cheng, Q.; Wei, T.; Farbiak, L.; Johnson, L. T.; Dilliard, S. A.; Siegwart, D. J. Selective organ targeting (SORT) nanoparticles for tissue-specific mRNA delivery and CRISPR−Cas gene editing. *Nat. Nanotechnol.* **2020**, *15*, 313−320.
(13) Miao, L.; Li, L.; Huang, Y.; Delcassian, D.; Chahal, J.; Han, J.; Shi, Y.; Sadtler, K.; Gao, W.; Lin, J.; Doloff, J. C.; Langer, R.; Anderson, D. G. Delivery of mRNA vaccines with heterocyclic lipids increases anti-tumor efficacy by STING-mediated immune cell activation. *Nat. Biotechnol.* **2019**, *37*, 1174−1185.
(14) Balwani, M.; Sardh, E.; Ventura, P.; Peiró, P. A.; Rees, D. C.; Stölzel, U.; Bissell, D. M.; Bonkovsky, H. L.; Windyga, J.; Anderson, K. E.; Parker, C.; Silver, S. M.; Keel, S. B.; Wang, J. D.; Stein, P. E.; Harper, P.; Vassiliou, D.; Wang, B.; Phillips, J.; Ivanova, A.; Langendonk, J. G.; Kauppinen, R.; Minder, E.; Horie, Y.; Penz, C.; Chen, J.; Liu, S.; Ko, J. J.; Sweetser, M. T.; Garg, P.; Vaishnaw, A.; Kim, J. B.; Simon, A. R.; Gouya, L. Phase 3 Trial of RNAi Therapeutic Givosiran for Acute Intermittent Porphyria. *N. Engl. J. Med.* **2020**, *382*, 2289−2301.
(15) Prakash, T. P.; Graham, M. J.; Yu, J.; Carty, R.; Low, A.; Chappell, A.; Schmidt, K.; Zhao, C.; Aghajan, M.; Murray, H. F.; Riney, S.; Booten, S. L.; Murray, S. F.; Gaus, H.; Crosby, J.; Lima, W. F.; Guo, S.; Monia, B. P.; Swayze, E. E.; Seth, P. P. Targeted delivery of antisense oligonucleotides to hepatocytes using triantennary N-acetyl galactosamine improves potency 10-fold in mice. *Nucleic Acids Res.* **2014**, *42*, 8796−8807.
(16) Zhang, J.; Salaita, K. *Smart Nucleic Acids as Future Therapeutics*. Trends Biotechnol. 2021, DOI: 10.1016/j.tibtech.2021.03.007.
(17) Zhang, J.; Ma, R.; Blanchard, A.; Petree, J.; Jo, H.; Salaita, K. Conditional Deoxyribozyme−Nanoparticle Conjugates for miRNA-Triggered Gene Regulation. *ACS Appl. Mater. Interfaces* **2020**, *12*, 37851−37861.
(18) Semenza, G. L. Targeting HIF-1 for cancer therapy. *Nat. Rev. Cancer* **2003**, *3*, 721−732.
(19) Semenza, G. L. HIF-1: upstream and downstream of cancer metabolism. *Curr. Opin. Genet. Dev.* **2010**, *20*, 51−56.
(20) Fernandez Esmerats, J.; Villa-Roel, N.; Kumar, S.; Gu, L.; Salim, M. T.; Ohh, M.; Taylor, W. R.; Nerem, R. M.; Yoganathan, A. P.; Jo, H. Disturbed Flow Increases UBE2C (Ubiquitin E2 Ligase C) via Loss of miR-483-3p, Inducing Aortic Valve Calcification by the pVHL (von Hippel-Lindau Protein) and HIF-1α (Hypoxia-Inducible Factor-1α) Pathway in Endothelial Cells. *Arterioscler., Thromb., Vasc. Biol.* **2019**, *39*, 467−481.
(21) Semenza, G. L. Hypoxia-inducible factor 1 and cardiovascular disease. *Annu. Rev. Physiol.* **2014**, *76*, 39−56.
(22) Gilkes, D. M.; Bajpai, S.; Chaturvedi, P.; Wirtz, D.; Semenza, G. L. Hypoxia-inducible factor 1 (HIF-1) promotes extracellular matrix remodeling under hypoxic conditions by inducing P4HA1, P4HA2, and PLOD2 expression in fibroblasts. *J. Biol. Chem.* **2013**, *288*, 10819−10829.
(23) Darby, I. A.; Hewitson, T. D. Hypoxia in tissue repair and fibrosis. *Cell Tissue Res.* **2016**, *365*, 553−562.
(24) Xiong, A.; Liu, Y. Targeting hypoxia inducible factors-1α as a novel therapy in fibrosis. *Front. Pharmacol.* **2017**, *8*, 326.
(25) Greenberger, L. M.; Horak, I. D.; Filpula, D.; Sapra, P.; Westergaard, M.; Frydenlund, H. F.; Albæk, C.; Schrøder, H.; Ørum, H. A RNA antagonist of hypoxia-inducible factor-1α, EZN-2968, inhibits tumor cell growth. *Mol. Cancer Ther.* **2008**, *7*, 3598−3608.
(26) Lagos-Quintana, M.; Rauhut, R.; Yalcin, A.; Meyer, J.; Lendeckel, W.; Tuschl, T. Identification of tissue-specific microRNAs from mouse. *Curr. Biol.* **2002**, *12*, 735−739.
(27) Landgraf, P.; Rusu, M.; Sheridan, R.; Sewer, A.; Iovino, N.; Aravin, A.; Pfeffer, S.; Rice, A.; Kamphorst, A. O.; Landthaler, M.; Lin, C.; Socci, N. D.; Hermida, L.; Fulci, V.; Chiaretti, S.; Foà, R.; Schliwka, J.; Fuchs, U.; Novosel, A.; Müller, R. U.; Schermer, B.; Bissels, U.; Inman, J.; Phan, Q.; Chien, M.; Weir, D. B.; Choksi, R.; de Vita, G.; Frezzetti, D.; Trompeter, H. I.; Hornung, V.; Teng, G.; Hartmann, G.; Palkovits, M.; di Lauro, R.; Wernet, P.; Macino, G.; Rogler, C. E.; Nagle, J. W.; Ju, J.; Papavasiliou, F. N.; Benzing, T.; Lichter, P.; Tam, W.; Brownstein, M. J.; Bosio, A.; Borkhardt, A.; Russo, J. J.; Sander, C.; Zavolan, M.; Tuschl, T. A mammalian microRNA expression atlas based on small RNA library sequencing. *Cell* **2007**, *129*, 1401−1414.
(28) Wienholds, E.; Kloosterman, W. P.; Miska, E.; Alvarez-Saavedra, E.; Berezikov, E.; de Bruijn, E.; Horvitz, H. R.; Kauppinen, S.; Plasterk, R. H. MicroRNA expression in zebrafish embryonic development. *Science* **2005**, *309*, 310−311.
(29) Lewis, A. P.; Jopling, C. L. Regulation and biological function of the liver-specific miR-122. *Biochem. Soc. Trans.* **2010**, *38*, 1553−1557.
(30) Bandiera, S.; Pfeffer, S.; Baumert, T. F.; Zeisel, M. B. miR-122−a key factor and therapeutic target in liver disease. *J. Hepatol.* **2015**, *62*, 448−457.
(31) Zhang, D. Y.; Seelig, G. Dynamic DNA nanotechnology using strand-displacement reactions. *Nat. Chem.* **2011**, *3*, 103.

https://doi.org/10.1021/acschembio.1c00387
ACS Chem. Biol. XXXX, XXX, XXX−XXX

(32) Post, D.; Van Meir, E. Generation of bidirectional hypoxia/HIF-responsive expression vectors to target gene expression to hypoxic cells. *Gene Ther.* **2001**, *8*, 1801−1807.
(33) Kehl, T.; Backes, C.; Kern, F.; Fehlmann, T.; Ludwig, N.; Meese, E.; Lenhof, H.-P.; Keller, A. About miRNAs, miRNA seeds, target genes and target pathways. *Oncotarget* **2017**, *8*, 107167.
(34) Rosen, M. A.; Live, D.; Patel, D. J. Comparative NMR study of An-bulge loops in DNA duplexes: intrahelical stacking of A, AA, and AAA bulge loops. *Biochemistry* **1992**, *31*, 4004−4014.
(35) Dornberger, U.; Hillisch, A.; Gollmick, F. A.; Fritzsche, H.; Diekmann, S. Solution structure of a five-adenine bulge loop within a DNA duplex. *Biochemistry* **1999**, *38*, 12860−12868.
(36) Tan, C.; de Noronha, R. G.; Devi, N. S.; Jabbar, A. A.; Kaluz, S.; Liu, Y.; Mooring, S. R.; Nicolaou, K.; Wang, B.; van Meir, E. G. Sulfonamides as a new scaffold for hypoxia inducible factor pathway inhibitors. *Bioorg. Med. Chem. Lett.* **2011**, *21*, 5528−5532.
(37) Chan, M. C.; Atasoylu, O.; Hodson, E.; Tumber, A.; Leung, I. K.; Chowdhury, R.; Gómez-Pérez, V.; Demetriades, M.; Rydzik, A. M.; Holt-Martyn, J.; Tian, Y. M.; Bishop, T.; Claridge, T. D. W.; Kawamura, A.; Pugh, C. W.; Ratcliffe, P. J.; Schofield, C. J. Potent and selective triazole-based inhibitors of the hypoxia-inducible factor prolyl-hydroxylases with activity in the murine brain. *PLoS One* **2015**, *10*, No. e0132004.
(38) Freier, S. M.; Altmann, K.-H. The ups and downs of nucleic acid duplex stability: structure-stability studies on chemically-modified DNA: RNA duplexes. *Nucleic Acids Res.* **1997**, *25*, 4429−4443.
(39) Nishina, K.; Piao, W.; Yoshida-Tanaka, K.; Sujino, Y.; Nishina, T.; Yamamoto, T.; Nitta, K.; Yoshioka, K.; Kuwahara, H.; Yasuhara, H.; Baba, T.; Ono, F.; Miyata, K.; Miyake, K.; Seth, P. P.; Low, A.; Yoshida, M.; Bennett, C. F.; Kataoka, K.; Mizusawa, H.; Obika, S.; Yokota, T. DNA/RNA heteroduplex oligonucleotide for highly efficient gene silencing. *Nat. Commun.* **2015**, *6*, 7969.
(40) Roloff, A.; Nelles, D. A.; Thompson, M. P.; Yeo, G. W.; Gianneschi, N. C. Self-transfecting micellar RNA: modulating nanoparticle cell interactions via high density display of small molecule ligands on micelle coronas. *Bioconjugate Chem.* **2018**, *29*, 126−135.
(41) Hum, J. M.; Siegel, A. P.; Pavalko, F. M.; Day, R. N. Monitoring biosensor activity in living cells with fluorescence lifetime imaging microscopy. *Int. J. Mol. Sci.* **2012**, *13*, 14385−14400.
(42) Feng, Y.-H.; Tsao, C.-J. Emerging role of microRNA-21 in cancer. *Biomed. Rep.* **2016**, *5*, 395−402.
(43) Graham, M. J.; Crooke, S. T.; Monteith, D. K.; Cooper, S. R.; Lemonidis, K. M.; Stecker, K. K.; Martin, M. J.; Crooke, R. M. In vivo distribution and metabolism of a phosphorothioate oligonucleotide within rat liver after intravenous administration. *J. Pharmacol. Exp. Ther.* **1998**, *286*, 447−458.

https://doi.org/10.1021/acschembio.1c00387
ACS Chem. Biol. XXXX, XXX, XXX−XXX